eter. Printer plots of several reflections using ω scans revealed a small peak on the left side of the main peaks. This was true of several crystals mounted. It was found that the whole peak could be collected by using a relatively large scan range of 2.2°. With this scan range, the data were collected in a standard manner. The space group $P2_12_12_1$ (No. 19) was uniquely determined by the following observed conditions: $h00$, $h = 2n$, $0k0$, $k = 2n$, and $00l$, $l = 2n$. No decay in the intensities of three standard reflections occurred. Data collection parameters are summarized in Table VI. The data were corrected for Lorentz and polarization effects.

Solution and Refinement of Structure. $Pb[(Ph_2P)_2CH]_2\cdot(C_2H_5)_2O$ (1). All structure determination calculations were done on a Data General Eclipse MV/10000 computer using the SHELXTL version 4 software package. The position of the lead and two of the phosphorus atoms were generated by direct methods. Other atom positions were located from successive difference Fourier maps. Anisotropic thermal parameters were assigned to the lead and phosphorus atoms, and isotropic thermal parameters were used for the remaining atoms. The final R value of 0.057 was computed from 272 least-square parameters and 1902 reflections. This yielded a goodness-of-fit of 1.22 and a mean shift/esd of 0.053 for rotation of the methyl group at C(54) on the last cycle of refinement. A value of 0.58 e/Å^3 (less than that expected for a hydrogen atom) was found as the largest feature on the final difference Fourier map. This peak was 1.24 Å from the tin atom. The weighting scheme used was $w = [\sigma^2(F_o)]^{-1}$. Correction for absorption were applied.[25] Neutral-atom scattering factors were those of Cromer and Waber.[26]

$Pb[(Ph_2P)_2C(SiMe_3)]_2$ (2). The position of the lead atom was found from the Patterson map. Other atom positions were located from successive difference Fourier maps. Anisotropic thermal parameters were assigned to lead, phosphorus, and silicon while isotropic thermal parameters were used for the remaining atoms. Refinement of these atoms converged at $R = 0.105$. The final stages of refinement included an absorption correction (XABS).[22] The handedness of the crystal was determined by use of a SHELXTL routine. This required inversion of the structure from the coordinates originally chosen. The correct hand converges with an R value of 0.053 while the incorrect one converges at an R value of 0.079. All hydrogen atoms were fixed at calculated positions by using a riding model in which the C–H vector was fixed at 0.98 Å, and the thermal parameter for each hydrogen atom was set at 1.2 times the value for the carbon atom to which it was bonded. A goodness-of-fit of 0.910 and a mean shift/esd of 0.006 for overall scale was calculated on the last cycle of refinement. A value of 0.97 e/Å^3 was found as the largest feature on the final difference Fourier map. This was 0.97 Å away from the lead atom and is probably a consequence of the relatively wide peaks of this crystal.

Acknowledgment. We thank the National Science Foundation (Grant CHE 8519557) for financial support. D.E.O. was a Earl C. Anthony Fellow.

Supplementary Material Available: A stereoview of **2** and listings of all bond lengths, bond angles, anisotropic thermal parameters, and hydrogen atom positional and thermal parameters for **1** and **2** (9 pages); listings of structure factor amplitudes for **1** and **2** (41 pages). Ordering information is given on any current masthead page.

(25) Hope, H.; Mozzi, B. "XABS, an absorption correction program producing an absorption tensor from an expression relating F_o and F_c"; Department of Chemistry, University of California, Davis, CA, unpublished results.

(26) *International Tables for X-ray Crystallography*; Kynoch: Birmingham, England, 1974; Vol. IV: (a) pp 149–150; (b) pp 99–101.

Contribution from the Chemistry and Materials Science Divisions, Argonne National Laboratory, Argonne, Illinois 60439, and Department of Chemistry, North Carolina State University, Raleigh, North Carolina 27650

Synthesis and Structure of ζ-$(BEDT\text{-}TTF)_2(I_3)(I_5)$ and $(BEDT\text{-}TTF)_2(I_3)(TlI_4)$: Comparison of the Electrical Properties of Organic Conductors Derived from Chemical Oxidation vs. Electrocrystallization

Mark A. Beno,*† Urs Geiser,† Kim L. Kostka,† Hau H. Wang,† Kevin S. Webb,† Millicent A. Firestone,† K. Douglas Carlson,† Luis Nuñez,† Myung-Hwan Whangbo,‡ and Jack M. Williams†

Received December 30, 1986

Chemical oxidation of bis(ethylenedithio)tetrathiafulvalene (BEDT-TTF or ET, $C_{10}S_8H_8$) in benzonitrile solution by slow diffusion of iodine vapor produces a mixture of black lustrous crystals. These include the well-known α- and β-$(ET)_2I_3$ phases, δ-$(ET)I_3$, and ϵ-$(ET)_2(I_3)(I_8)_{0.5}$, as well as a new phase, ζ-$(ET)_2(I_3)(I_5)$. Single-crystal X-ray diffraction studies show that this latter salt is monoclinic, $P2_1/a$, with $a = 15.113$ (4) Å, $b = 15.993$ (6) Å, $c = 18.159$ (9) Å, $\beta = 100.99$ (3)°, $V_c = 4308$ (2) Å^3, and $Z = 4$. The crystal structure consists of two-dimensional sheets containing both ET donor molecules and I_3^- anions, and these mixed ET–I_3^- sheets are separated by layers of V-shaped I_5^- anions. This ζ-phase is structurally very similar to ϵ-$(ET)_2(I_3)(I_8)_{0.5}$. Four-probe resistivity measurements of single crystals of ϵ-$(ET)_2(I_3)(I_8)_{0.5}$ and ζ-$(ET)_2(I_3)(I_5)$ both prepared by the present chemical oxidation method show that, although these materials are metallic to temperatures as low as 1.7 K, they do not undergo transitions to the superconducting state. These findings were confirmed by radio-frequency (rf) field penetration depth measurements of the same samples, which failed to detect superconductivity down to temperatures of 0.5 K. Band electronic structure calculations based on the crystal structure parameters of ϵ-$(ET)_2(I_3)(I_8)_{0.5}$ and ζ-$(ET)_2(I_3)(I_5)$ predict semiconducting properties for stoichiometric crystals. Therefore, it is proposed that the observed metallic properties result from the presence of anion vacancies producing slightly nonstoichiometric crystals. A new salt $(ET)_2(I_3)(TlI_4)$ was prepared by electrochemical oxidation, and a crystal structure study reveals that it is monoclinic, $P2_1/n$, with $a = 8.348$ (3) Å, $b = 15.294$ (8) Å, $c = 34.217$ (16) Å, $\beta = 93.61(3)$°, $V_c = 4360$ (3) Å^3, and $Z = 4$. As in the case of ϵ-$(ET)_2(I_3)(I_8)_{0.5}$ and δ-$(ET)_2(I_3)(I_5)$, $(ET)_2(I_3)(TlI_4)$ consists of mixed two-dimensional sheets containing both ET donor molecules and I_3^- anions, which are separated by layers of tetrahedral TlI_4^- ions. The salt is a semiconductor, in agreement with our band structure calculations.

Introduction

Electrolytic oxidation of bis(ethylenedithio)tetrathiafulvalene[1] (BEDT-TTF or ET, $C_{10}S_8H_8$) in the presence of triiodide anions leads to the ambient-pressure organic superconductors β-$(ET)_2I_3$ (superconducting transition temperature $T_c = 1.5$ K)[2,3] and γ-$(ET)_3(I_3)_{2.5}$ ($T_c = 2.5$ K),[4,5] as well as nonsuperconducting α-$(ET)_2I_3$[6] and δ-$(ET)I_3$.[5] Of these salts, the δ- and γ-phases are reportedly synthesized by electrocrystallization in 1,1,2-tri-

(1) Williams, J. M.; Beno, M. A.; Wang, H. H.; Leung, P. C. W.; Emge, T. J.; Geiser, U.; Carlson, K. D. *Acc. Chem. Res.* **1985**, *18*, 261.
(2) Yagubskii, E. B.; Shchegolev, I. F.; Laukhin, V. N.; Kononovich, P. A.; Kartsovnik, M. V.; Zvarykina, A. V.; Buravov, L. I. *JETP Lett.* (*Engl. Transl.*) **1984**, *39*, 12.
(3) Williams, J. M.; Emge, T. J.; Wang, H. H.; Beno, M. A.; Copps, P. T.; Hall, L. N.; Carlson, K. D.; Crabtree, G. W. *Inorg. Chem.* **1984**, *23*, 2558.

† Argonne National Laboratory.
‡ North Carolina State University.

0020-1669/87/1326-1912$01.50/0

Table I. Summary of Crystallographic and ESR Data for ET Salts Derived by Chemical Oxidation

compd	description	space group	a, Å	b, Å	c, Å	α, deg	β, deg	γ, deg	unit cell vol., Å^3	Z	av ESR line width, G	ref
α-$(ET)_2I_3$	thick rhombohedron and thin irregular plates	$P\bar{1}$	9.011	10.850	17.488	96.95	97.97	90.75	1717	2	76–100	3, 6
β-$(ET)_2I_3$	thick distorted hexagon crystals	$P\bar{1}$	6.615	9.100	15.286	94.38	95.5	109.78	855.9	1	20–23	2, 3
δ-$(ET)I_3$	thin needle crystals	$C2/c$	10.728	34.14	34.92	95.00	90	90	12736	24	ESR inactive	5
ε-$(ET)_2(I_3)(I_8)_{0.5}$	thick needle crystals	$P2_1/a$	17.458	14.035	18.808	90	112.70	90	4251	4	ESR inactive	7[a]
ζ-$(ET)_2(I_3)(I_5)$	rectangular thin plates	$P2_1/a$	15.133	15.993	18.159	90	100.99	90	4309	4	ESR inactive	this work

[a] Lattice constants as measured for this work (supplementary Table XI). Reference 7 gives a different setting of the space group.

chloroethane solution at high current densities (~65 μA/cm^2).[5] Chemical oxidation of ET by I_2 leads to ε-$(ET)_2(I_3)(I_8)_{0.5}$, which was initially reported to be a superconductor[5,18] but later found to be a nonsuperconductor.[7] The electrical properties of the α- and β-$(ET)_2I_3$ materials have been confirmed,[2,5,7,8] but those of γ-$(ET)_3(I_3)_{2.5}$ and ε-$(ET)_2(I_3)(I_8)_{0.5}$ have not been confirmed yet because of difficulties in synthesizing these materials by electrolytic oxidation. In the present study we report our procedure for the synthesis of ET charge-transfer salts by chemical oxidation, which produces crystals of a new metallic phase ζ-$(ET)_2(I_3)(I_5)$ as well as ε-$(ET)_2(I_3)(I_8)_{0.5}$. The crystal structures of two salts δ-$(ET)_2(I_3)(I_5)$ and $(ET)_2(I_3)(TlI_4)$, the latter being a semiconducting derivative synthesized by electrochemical oxidation, are presented here along with a model for the occurrence of conducting behavior in these materials.

The structures of ζ-$(ET)_2(I_3)(I_5)$, ε-$(ET)_2(I_3)(I_8)_{0.5}$, and $(ET)_2(I_3)(TlI_4)$, as determined by single-crystal X-ray diffraction in the present study, show that these salts are structurally similar. The ζ- and ε-phases are metallic down to 1.7 K but are not bulk superconductors down to 0.5 K, while $(ET)_2(I_3)(TlI_4)$ is semiconducting. Tight-binding-band electronic structure calculations for ζ-$(ET)_2(I_3)(I_5)$ and ε-$(ET)_2(I_3)(I_8)_{0.5}$ reveal that these salts cannot be metallic if they are as stoichiometric as their chemical formulas indicate, and it would appear that their metallic nature is likely due to the presence of anion vacancies.

Experimental Section

Chemical Oxidation of ET. Benzonitrile was dried overnight over CaH_2 and then $CaCl_2$ and subsequently stirred over P_2O_5 for 4 days. The solvent was then vacuum-distilled and collected over argon. Immediately before use, the distilled solvent was passed through an Al_2O_3 column. An orange solution of ET in benzonitrile was prepared by adding 14.6 mg of ET (Strem Chemical Co.) to 15 mL of dry benzonitrile (2.5 mM) with mild heating and stirring under argon. This solution was transferred to a beaker that was purged with argon and sealed with two layers of Parafilm. Two small pinholes were punched in the film, and the beaker was placed in a desiccator containing iodine crystals (Aldrich, Gold Label) with no desiccant, which was maintained at a constant temperature of 22.3 ± 0.2 °C and allowed to stand undisturbed. Lustrous black crystals first appeared overnight. After 7 days, the dark solution was suction-filtered and the black crystals were washed with dry THF. A total mass of ~25 mg of product was formed, which contained many different crystalline morphologies: viz., thin needles of δ-$(ET)I_3$, thick distorted hexagons of β-$(ET)_2I_3$, thick rhombohedrons and thin irregular plates of α-$(ET)_2I_3$, thick needles of ε-$(ET)_2(I_3)(I_8)_{0.5}$, and rectangular thin plates of ζ-$(ET)_2(I_3)(I_5)$, which were all identified by their room-temperature ESR line widths and unit cell parameters, as summarized in Table I.

Electrocrystallization of $(ET)_2(I_3)(TlI_4)$. In an attempt to prepare a possible "TlI_2^-" anion, $(n\text{-}Bu)_4NTlI_4$ and Tl turnings were mixed together in a 1:2.4 molar ratio, respectively, and refluxed over methylene chloride for 4 days. Most of the starting material was recovered without change, but the third crop of the soluble butylammonium salt from the reaction mixture gave a lower and sharp melting point (125–126 °C) and a much lighter color. Electrocrystallization with ET was carried out in THF solvent as in the literature[26] by using 8.4 mg of ET (1.5 mM) and 87 mg of the above butylammonium salt, which was characterized by elemental analysis as $(n\text{-}Bu)_4NTlI_4$ contaminated with $(n\text{-}Bu)_4NI$. A 3.1-mg sample of black shiny crystals was harvested after 5 days of crystal growth under a constant current density of 2.7 μA/cm^2 at 23.0 ± 0.2 °C to give a 23% yield. The composition of this new mixed-anion material, $(ET)_2(I_3)(TlI_4)$, was derived from the crystal structure determination.

X-ray Diffraction. The details of the X-ray diffraction experiments of ζ-$(ET)_2(I_3)(I_5)$ and $(ET)_2(I_3)(TlI_4)$ are presented in Table II. The unit cell lattice parameters were obtained from the setting angles of 25

(4) Yagubskii, E. B.; Shchegolev, I. F.; Pesotskii, S. I.; Laukhin, V. N.; Kononovich, P. A.; Kartsovnik, M. V.; Zvarykina, A. V. *JETP Lett. (Engl. Transl.)* **1984**, *39*, 328.
(5) Shibaeva, R. P.; Kaminskii, V. F.; Yagubskii, E. B. *Mol. Cryst. Liq. Cryst.* **1985**, *119*, 361.
(6) Bender, K.; Hennig, I.; Schweitzer, D.; Dietz, K.; Endres, H.; Keller, H. J. *Mol. Cryst. Liq. Cryst.* **1984**, *108*, 359.
(7) Shibaeva, R. P.; Lobkovskaya, R. M.; Yagubskii, E. B.; Kostyuchenko, E. Z. *Kristallografiya* **1986**, *31*, 455.
(8) Yagubskii, E. B.; Shchegolev, I. F.; Laukhin, V. N.; Shibaeva, R. P.; Kostyuchenko, E. E.; Khomenko, A. G.; Sushko, Yu. V.; Zvarykina, A. V. *JETP Lett. (Engl. Transl.)* **1984**, *40*, 1201.
(9) Main, P.; Hull, S. E.; Lessinger, L.; Germain, G.; Declercq, J.-P.; Woolfson, M. M. "MULTAN78. A System of Computer Programs for the Automatic Solution of Crystal Structures from X-Ray Diffraction Data"; Universities of York, England, and Louvain, Belgium, 1978.
(10) *International Tables for X-Ray Crystallography*; Kynoch: Birmingham, England, 1978; Vol. IV.
(11) Strouse, C. "UCLA Crystallographic Program Package"; University of California, Los Angeles, 1978.
(12) (a) Broekema, J.; Havinga, H. H.; Wiebenga, E. H. *Acta Crystallogr.* **1957**, *10*, 596. (b) Hon, P. K.; Thomas, C. W.; Trotter, J. *Inorg. Chem.* **1979**, *10*, 2916 and references therein.
(13) Since the molecular planes of the two independent ET molecules of a dimer unit are nonparallel (3.4° dihedral angle), the interplanar spacing for the ε-phase salt was estimated by the average distance from the plane defined by the four inner (TTF portion) sulfur atoms of molecule A to the corresponding plane of molecule B.
(14) Kobayashi, H.; Kobayashi, A.; Sasaki, Y.; Saito, G.; Inokuchi, H. *Bull. Chem. Soc. Jpn.* **1986**, *59*, 301.
(15) (a) Kobayashi, H.; Kato, R.; Mori, T.; Kobayashi, A.; Sasaki, Y.; Saito, G.; Enoki, T.; Inokuchi, H. *Chem. Lett.* **1984**, 179. (b) Kanbara, H.; Tajima, H.; Aratani, S.; Yakushi, K.; Kuroda, H.; Saito, G.; Kawamoto, A.; Tanaka, J. *Chem. Lett.* **1986**, 437. (c) Beno, M. A.; Blackman, G. S.; Leung, P. C. W.; Carlson, K. D.; Copps, P. T.; Williams, J. M. *Mol. Cryst. Liq. Cryst.* **1985**, *119*, 409.
(16) (a) Kobayashi, H.; Kobayashi, A.; Sasaki, Y.; Saito, G.; Inokuchi, H. *Chem. Lett.* **1984**, 183. (b) Geiser, U.; Wang, H. H.; Gerdom, L. E.; Firestone, M. A.; Sowa, L. M.; Williams, J. M.; Whangbo, M.-H. *J. Am. Chem. Soc.* **1985**, *107*, 8305.
(17) Carlson, K. D.; Crabtree, G. W.; Hall, L. N.; Copps, P. T.; Wang, H. H.; Emge, T. J.; Beno, M. A.; Williams, J. M. *Mol. Cryst. Liq. Cryst.* **1985**, *119*, 357.
(18) Merzhanov, V. A.; Kostyuchenko, E. E.; Laukhin, V. N.; Lobkovskaya, R. M.; Makova, M. K.; Shibaeva, R. P.; Shchegolev, I. F.; Yagubski, E. B. *JETP Lett. (Engl. Transl.)* **1985**, *41*, 179.
(19) Crabtree, G. W.; Carlson, K. D.; Hall, L. N.; Copps, P. T.; Wang, H. H.; Emge, T. J.; Beno, M. A.; Williams, J. M. *Phys. Rev. B: Condens. Matter* **1984**, *30*, 2958.
(20) Thiele, G.; Rotter, H. W.; Zimmerman, K. *Z. Naturforsch., B: Anorg. Chem., Org. Chem.* **1986**, *41B*, 269.
(21) Whangbo, M.-H.; Williams, J. M.; Leung, P. C. W.; Beno, M. A.; Emge, T. J.; Wang, H. H. *Inorg. Chem.* **1985**, *24*, 3500.
(22) Whangbo, M.-H.; Williams, J. M.; Leung, P. C. W.; Beno, M. A.; Emge, T. J.; Wang, H. H.; Carlson, K. D.; Crabtree, G. W. *J. Am. Chem. Soc.* **1985**, *107*, 5815.
(23) We used double-ζ Slater type orbitals adapted from: Clementi, E.; Roetti, C. *At. Data Nucl. Data Tables* **1974**, *14*, 177. The $H_{\mu\mu}$ values were calculated from a modified Wolfsberg–Helmholtz formula: Ammeter, J. H.; Bürgi, H.-B.; Thibeault, J. C.; Hoffmann, R. *J. Am. Chem. Soc.* **1978**, *100*, 3686. For details, see ref 19.
(24) Hoffmann, R. *J. Chem. Phys.* **1963**, *39*, 1397.
(25) Whangbo, M.-H. In *Crystal Chemistry and Properties of Materials with Quasi One-Dimensional Structures*; Rouxel, J., Ed.; Reidel: Dordrecht, The Netherlands, 1986; p 27.
(26) Stephens, D. A.; Rehan, A. E.; Compton, S. J.; Barkhau, R. A.; Williams, J. M. *Inorg. Synth.* **1986**, *24*, 135.

Table II. Experimental Parameters for the X-ray Diffraction Study

ζ-$(ET)_2(I_3)(I_5)$

A. Crystal Parameters

space group, $P2_1/a$ [C_{2h}^5, no. 14]	γ = 0.71073 Å (Mo Kα; graphite monochromator)
cell constants	M_r = 1784.610
a = 15.113 (4) Å	ρ_c = 2.751 g/cm^3
b = 15.993 (6) Å	μ_c = 64.72 cm^{-1}
c = 18.159 (9) Å	T_{min} = 0.59, T_{max} = 0.99
β = 100.99 (3)°	cryst dimens: 0.48 × 0.42 × 0.034 mm
V_{cell} = 4309 (2) Å^3	
Z = 4 formula units/unit cell	

B. Measurement of Intensity Data

no. of total reflcns	18481 on Nicolet $P2_1$
data collecn mode	ω scans, 1.0–12.0°/min
no. of total unique reflcns	9971, 8438 with $F_o^2 > 0.0$
no. of reflcns with $F^2 \geq 3\sigma(F^2)$	6500
$(\sin\theta_{max})/\lambda$	0.65 Å^{-1} ($4.0° \leq 2\theta \leq 55.0°$)
agreement factors for averaging	$R_{av}(F)$ = 0.11, $R_{w,av}(F)$ = 0.05[b]
no. of data to param ratio	25 (all data), 16.4 ($F^2 \geq 3\sigma(F^2)$)
function minimized	$\sum w(\lvert F_o\rvert - \lvert F_c\rvert)^2$ where $w = 1/\sigma(F_o)^2$ and $\sigma(F_o) = (1/(2F_o))[\sigma(F_o^2)^2 + (0.02F_o^2)^2]^{1/2}$

C. Agreement Factors[a]

	data with $F_o > 0.0$	data with $F_o^2 \geq 3\sigma(F^2)$
$R(F_o)$	0.107	0.087
$R_w(F_o)$	0.083	0.081
goodness-of-fit	2.072	2.241

$(ET)_2(I_3)(TlI_4)$

A. Crystal Parameters

space group $P2_1/n$ [C_{2h}^5, No. 14]	λ = 0.71073 Å (Mo Kα; graphite monochromator)
cell constants	M_r = 1862.07
a = 8.348 (3) Å	ρ_c = 2.84 g/cm^3
b, = 15.294 (8) Å	μ_c = 94.1 cm^{-1}
c = 34.217 (16) Å	T_{min} = 0.27, T_{max} = 0.75
β = 93.61 (3)°	cryst dimens: 0.15 × 0.45 × 0.03 mm
V_{cell} = 4360 (3) Å	
Z = 4 formula units/unit cell	

B. Measurement of Intensity Data

no. of total reflcns	8710 on Nicolet P3/F
data collecn mode	ω scans, 1.0–12.0°/min
no. of total unique reflcns	7662
no. of reflcns with $F \geq 3\sigma(F)$	4874
$(\sin\theta_{max})/\lambda$	0.595 Å^{-1} ($4.0 \leq 2\theta \leq 50.0°$)
agreement factors for averaging	$R_{av}(F)$ = 0.047, $R_{w,av}(F)$ = 0.25[b]
data to param ratio	19 (all data), 12 ($F \geq 3\sigma(F)$)
function minimized	$\sum w(\lvert F_o\rvert - \lvert F_c\rvert)^2$ where $w = 1/\sigma(F_o)^2$ and $\sigma(F_o) = (1/(2F_o))[\sigma(F_o^2)^2 + (0.02F_o^2)^2]^{1/2}$

C. Agreement Factors[a]

	data with $F_o > 0.0$	data with $F_o \geq 3\sigma(F)$
$R(F_o)$	0.094	0.069
$R_w(F_o)$	0.050	0.048
goodness-of-fit	1.616	1.721

[a] $R(F_o) = \sum\lvert\lvert F_o\rvert - \lvert F_c\rvert\rvert/\sum\lvert F_o\rvert$, $R_w(F_o) = [\sum w(\lvert F_o\rvert - \lvert F_c\rvert)^2/\sum w\lvert F_o\rvert^2]^{1/2}$, "goodness-of-fit" = $[\sum w(\lvert F_o\rvert - \lvert F_c\rvert)^2/(n-m)]$ for n observations and m = 397 (ζ-$(ET)_2(I_3)(I_5)$) or 398 ($(ET)_2(I_3)(TlI_4)$) variable parameters. [b] $R_{av}(F_o) = \sum\lvert F_o - F_{av}\rvert/\sum F_o$, $R_{w,av}(F_o) = [\sum w(F_o - F_{av})^2/\sum wF_o^2]^{1/2}$.

centered reflections. Intensity data were corrected for Lorentz and polarization effects, and a Gaussian absorption correction was applied. The structures were solved by using MULTAN78[9] and refined by use of full-matrix least-squares procedures. For ζ-$(ET)_2(I_3)(I_5)$, anisotropic temperature factors were used for all non-hydrogen atoms with the exception of the disordered ethylene group carbon atoms [C(10) and C(20)] of the ET molecule. Because of the large observed thermal parameters, it was concluded that each of the two independent ET molecules has one disordered ethylene group. One of the two carbon atoms in each disordered ethylene group has a site separation too small to refine, assuming two separate positions [C(9) and C(19)]. However, the other carbon atoms of each disordered ethylene group were refined into two separate positions, and site occupations were determined [C(10A) and C(10B); C(20A) and C(20B)]. For $(ET)_2(TlI_4)(I_3)$, all non-hydrogen atoms were refined with anisotropic thermal parameters, and hydrogen atoms were fixed at their calculated positions. The atomic and anomalous-scattering factors were taken from ref 10. All computations were carried out by using a local modification of the UCLA Crystallographic Program Package.[11] The refined positional parameters are given in Tables III and IV, and the anisotropic thermal parameters and calculated and observed structure factors are deposited as supplementary material.

Table III. Final Atomic Positional and Thermal Parameters of ζ-$(ET)_2(I_5)(I_3)$

atom	x	y	z	10^4U_{eq}[a]
I(1)	0.28245 (7)	0.26678 (8)	1.13153 (7)	626 (4)
I(2)	0.22528 (6)	0.28104 (6)	0.96839 (6)	485 (3)
I(3)	0.16898 (7)	0.30152 (7)	0.80822 (7)	582 (4)
I(4)	−0.11827 (8)	0.13169 (8)	0.38659 (8)	706 (5)
I(5)	−0.21919 (7)	0.25814 (7)	0.43724 (6)	480 (3)
I(6)	−0.32527 (8)	0.40077 (8)	0.49585 (6)	586 (4)
I(7)	−0.18810 (8)	0.53370 (7)	0.46636 (6)	603 (4)
I(8)	−0.0675 (2)	0.65431 (12)	0.43587 (10)	1183 (8)
S(1)	0.9680 (2)	0.1336 (2)	0.0453 (2)	366 (11)
S(2)	1.1411 (2)	0.0611 (2)	0.0332 (2)	372 (11)
S(3)	1.0941 (2)	0.0777 (2)	−0.1447 (2)	380 (11)
S(4)	0.9162 (2)	0.1435 (2)	−0.1371 (2)	359 (11)
S(5)	0.9979 (2)	0.1298 (2)	0.2093 (2)	406 (11)
S(6)	1.2040 (2)	0.0393 (2)	0.1943 (2)	371 (11)
S(7)	1.0655 (2)	0.0749 (3)	−0.3099 (2)	482 (13)
S(8)	0.8505 (2)	0.1430 (3)	−0.3007 (2)	441 (12)
C(1)	1.0384 (9)	0.0993 (8)	−0.0123 (8)	388 (45)
C(2)	1.0177 (7)	0.1051 (8)	−0.0915 (7)	277 (37)
C(3)	1.0386 (8)	0.1085 (8)	0.1271 (7)	302 (40)
C(4)	1.1201 (7)	0.0735 (8)	0.1234 (7)	266 (37)
C(5)	1.0219 (8)	0.0957 (8)	−0.2314 (7)	317 (40)
C(6)	0.9386 (9)	0.1243 (8)	−0.2250 (7)	355 (43)
C(7)	1.0905 (10)	0.0997 (10)	0.2851 (7)	432 (48)
C(8)	1.1843 (11)	0.1100 (10)	0.2666 (9)	491 (53)
C(9)	0.9172 (13)	0.1676 (15)	−0.3744 (9)	783 (80)
C(10A)[b]	0.9984 (33)	0.1507 (38)	−0.3710 (28)	386 (180)
C(10B)	0.9763 (13)	0.1030 (15)	−0.3867 (11)	334 (76)
S(11)	0.8371 (2)	0.4876 (3)	−0.0595 (2)	427 (12)
S(12)	0.9721 (2)	0.3617 (2)	−0.0738 (2)	427 (12)
S(13)	1.0302 (2)	0.3531 (2)	0.1068 (2)	428 (12)
S(14)	0.8942 (2)	0.4780 (3)	0.1194 (2)	440 (12)
S(15)	0.7662 (2)	0.5060 (2)	−0.2196 (2)	442 (12)
S(16)	0.9226 (3)	0.3480 (3)	−0.2380 (2)	529 (14)
S(17)	1.0933 (3)	0.3354 (2)	0.2717 (2)	464 (13)
S(18)	0.9286 (3)	0.4778 (3)	0.2857 (2)	572 (15)
C(11)	0.9231 (8)	0.4235 (9)	−0.0149 (8)	373 (44)
C(12)	0.9462 (9)	0.4189 (9)	0.0634 (9)	434 (50)
C(13)	0.8419 (8)	0.4549 (9)	−0.1489 (7)	372 (45)
C(14)	0.9021 (9)	0.3953 (8)	−0.1553 (7)	359 (43)
C(15)	1.0208 (9)	0.3832 (9)	0.1989 (7)	373 (45)
C(16)	0.9545 (9)	0.4400 (9)	0.2030 (8)	410 (47)
C(17)	0.7981 (10)	0.4651 (9)	−0.3046 (8)	418 (47)
C(18)	0.8198 (11)	0.3733 (10)	−0.2997 (8)	521 (55)
C(19)	1.0166 (16)	0.3307 (14)	0.3408 (12)	876 (87)
C(20A)[b]	0.9820 (19)	0.4118 (19)	0.3598 (16)	545 (102)
C(20B)	0.9467 (29)	0.3740 (29)	0.3312 (25)	397 (160)

[a] The complete temperature factor is $\exp[-8\pi^2U_{eq}(\sin^2\theta)/(\lambda^2)]$ where $U_{eq} = {}^1/_3\sum_i\sum_j U_{ij}a^*_i a^*_j \mathbf{a}_i\cdot\mathbf{a}_j$ in units of Å^2. [b] The refined populations of the A and B sites are 0.311 and 0.689 for C(10) and 0.642 and 0.358 for C(20).

To facilitate comparison of the ϵ- and ζ-phases uniquely obtained herein by chemical oxidation, room-temperature X-ray diffraction data were also obtained for ϵ-$(ET)_2(I_3)(I_8)_{0.5}$. The unit cell and refined positional and thermal parameters for the ϵ-phase crystal, which are in excellent agreement with those reported by Shibaeva et al.,[7] are included as supplementary material.

Electrical Property Measurements. Four-probe resistivity measurements in the temperature range 300–1.7 K were carried out on single crystals of ϵ-$(ET)_2(I_3)(I_8)_{0.5}$ and ζ-$(ET)_2(I_3)(I_5)$ with the use of low-frequency ac current (50 μA at ~37 Hz) and phase-sensitive detection of the voltage drop. The resistivities were measured along the needle axis a for the ϵ-phase crystal and crystallographic c axis for the ζ-phase crystal. The electrical leads consisted of fine gold wire (12.7 μm) attached to the crystals with gold conducting paste. The resistivity for both phases indicates metallic conductivity throughout the temperature range, as displayed in Figure 1. The ϵ-phase shows a noticeable decrease in resistivity near 7 K, somewhat similar to, but much less pronounced than,

Table IV. Final Atomic Positional and Thermal Parameters of $(ET)_2(I_3)(TlI_4)$

atom	x	y	z	10^4U_{eq}[a]
Tl	0.04305 (7)	0.20619 (4)	0.23655 (2)	494 (2)
I(1)	0.06247 (13)	0.22515 (7)	0.15687 (3)	579 (4)
I(2)	−0.2139 (2)	0.29916 (11)	0.26081 (4)	975 (7)
I(3)	0.32707 (15)	0.26459 (10)	0.27142 (4)	880 (6)
I(4)	−0.0068 (3)	0.03210 (9)	0.25177 (5)	1236 (8)
I(5)	0.2267 (2)	0.21215 (8)	0.39109 (4)	715 (5)
I(6)	0.39685 (13)	0.22658 (7)	0.46781 (3)	573 (4)
I(7)	0.5570 (2)	0.24403 (8)	0.54565 (4)	737 (5)
S(1)	0.6748 (5)	0.0546 (3)	−0.07583 (12)	565 (17)
S(2)	0.5409 (6)	−0.1202 (3)	−0.07416 (13)	603 (18)
S(3)	0.7876 (5)	0.0397 (3)	0.01525 (13)	582 (17)
S(4)	0.6425 (6)	−0.1334 (3)	0.01837 (13)	552 (17)
S(5)	0.6100 (7)	0.0811 (3)	−0.16054 (14)	798 (22)
S(6)	0.4348 (7)	−0.1236 (3)	−0.15837 (14)	725 (20)
S(7)	0.9128 (6)	0.0435 (3)	0.09649 (13)	653 (18)
S(8)	0.7362 (6)	−0.1651 (3)	0.10077 (14)	655 (19)
C(1)	0.6345 (17)	−0.0366 (10)	−0.0484 (4)	445 (58)
C(2)	0.6756 (19)	−0.0422 (10)	−0.0098 (5)	561 (67)
C(3)	0.5963 (18)	0.0137 (10)	−0.1200 (4)	448 (58)
C(4)	0.5307 (19)	−0.0665 (9)	−0.1191 (4)	467 (60)
C(5)	0.8122 (18)	−0.0142 (9)	0.0593 (4)	451 (57)
C(6)	0.7380 (19)	−0.0950 (9)	0.0608 (4)	469 (60)
C(7)	0.5899 (32)	0.0056 (15)	−0.2004 (6)	1267 (125)
C(8)	0.5075 (35)	−0.0660 (14)	−0.1995 (5)	1270 (124)
C(9)	0.9038 (23)	−0.0293 (12)	0.1373 (5)	815 (86)
C(10)	0.8998 (23)	−0.1198 (12)	0.1307 (5)	774 (83)
S(11)	0.0147 (5)	0.1503 (2)	0.52703 (12)	436 (14)
S(12)	−0.1980 (5)	0.0134 (3)	0.55270 (11)	438 (14)
S(13)	−0.1231 (5)	0.1308 (2)	0.44012 (12)	510 (16)
S(14)	−0.3411 (5)	−0.0067 (3)	0.46100 (11)	431 (14)
S(15)	0.1648 (5)	0.1927 (3)	0.60362 (13)	546 (16)
S(16)	−0.0976 (6)	0.0336 (3)	0.63728 (12)	597 (17)
S(17)	−0.2300 (6)	0.1362 (3)	0.35621 (13)	708 (20)
S(18)	−0.4902 (5)	−0.0313 (3)	0.38173 (12)	519 (16)
C(11)	−0.1330 (17)	0.0742 (9)	0.5143 (4)	373 (52)
C(12)	−0.1963 (16)	0.0667 (8)	0.4765 (4)	351 (53)
C(13)	0.0203 (16)	0.1289 (9)	0.5764 (4)	401 (55)
C(14)	−0.0789 (16)	0.0656 (9)	0.5886 (4)	374 (53)
C(15)	−0.2491 (18)	0.0899 (9)	0.4015 (4)	412 (57)
C(16)	−0.3482 (17)	0.0248 (9)	0.4113 (4)	416 (55)
C(17)	0.1446 (21)	0.1535 (10)	0.6523 (5)	633 (71)
C(18)	−0.0242 (18)	0.1316 (10)	0.6617 (5)	499 (61)
C(19)	−0.3725 (32)	0.0823 (19)	0.3265 (6)	1586 (142)
(20)	−0.5068 (21)	0.0359 (12)	0.3380 (5)	688 (74)

[a] The complete temperature factor is $\exp[-8\pi^2U_{eq}(\sin^2\theta)/\lambda^2]$ where $U_{eq} = {}^1/_3\sum_{ij}U_{ij}a_i^*a_j^*\mathbf{a}_i\mathbf{a}_j$ in units of Å^2.

the sharp resistance decrease near 8 K at ambient pressure reported for the superconducting β-$(ET)_2I_3$ phase.[17] Also similar to that of the β-phase, the resistivity vs. T plot for the ϵ-phase is approximately linear in the temperature range 300–100 K and shows a somewhat steeper slope in the ranges 100–10 K and 7–1.7 K. The resistivity below 7 K shows no indication of a superconducting transition. The resistivity of the ζ-phase shows an unusual leveling off in the region 135–115 K. This may be an artifact of the measurement, but this behavior was found to be reproducible on repeated thermal cycling. The resistivity of the ζ-phase, as illustrated in Figure 1, exhibits a slight decrease near 4.5 K, but there is no evidence of a transition to a superconducting state above 1.7 K. The resistivity ratios $R_{300}/R_{1.7}$ are ~130 for the ϵ-phase specimen and ~50 for the ζ-phase specimen. From the crystal dimensions and voltage-probe distances, it is estimated that the conductivities at 300 K are ~1 and 0.1 $(\Omega\ cm)^{-1}$ for the ϵ- and ζ-phase crystals with dimensions of ~0.5 × 0.2 × 0.05 mm and 0.5 × 0.3 × 0.1 mm, respectively. Additional samples taken from the same batches produced similar results.

Four-probe resistivity measurements on single crystals of $(ET)_2(I_3)(TlI_4)$ were carried out by the same technique as described above, but with an ac current of 30 μA at 37 Hz. The contacts were mounted along an arbitrary direction within the crystallographic *ab* plane. The resistivity increased exponentially with decreasing temperatures. The lowest temperature measured was 170 K. An activation energy, E_a, of 0.07 eV is derived from the plot of ln R vs. $1/T$, and a room-temperature conductivity of ca. 0.01 $(\Omega\ cm)^{-1}$ from the approximate crystal dimensions.

Tests for bulk superconductivity in the ϵ- and ζ-phase crystals at temperatures down to 0.5 K were carried out by rf penetration depth measurements with the use of equipment and procedures described previously.[19] These measurements have a high sensitivity to changes in the resonant frequency of the rf coil (1 Hz in 10^5 Hz) due to the exclusion of the field by the persistent shielding currents, when a sample becomes a superconductor, and are capable of detecting superconductivity in as little as 10 μg of an organic superconductor.[17] The samples tested consisted of several hundred micrograms of the ϵ- and δ-phase crystals. No frequency change indicative of superconductivity was observed in these experiments down to 0.5 K.

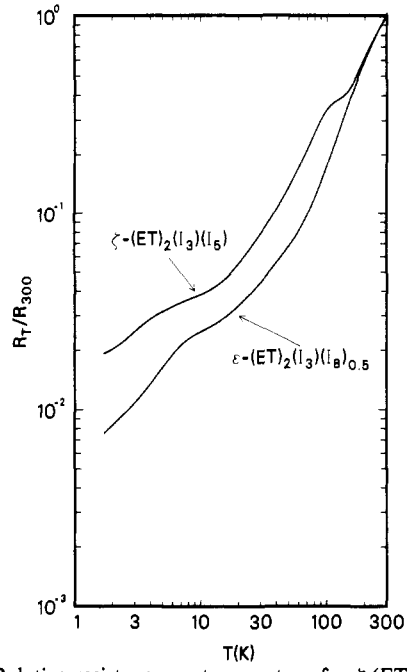

Figure 1. Relative resistance vs. temperature for ζ-$(ET)_2(I_3)(I_5)$ and ϵ-$(ET)_2(I_3)(I_8)_{0.5}$ as obtained by four-probe resistivity measurements, showing that both salts are metallic to 1.7 K.

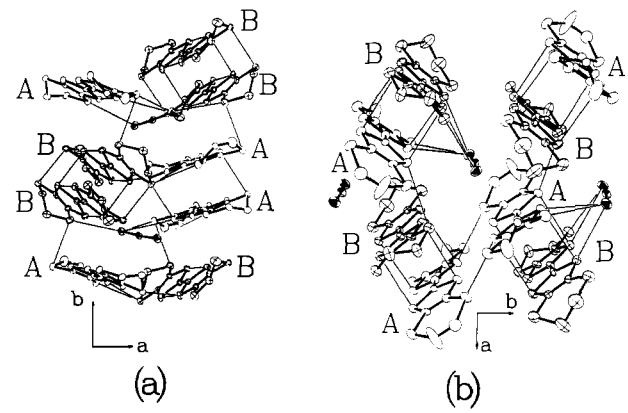

Figure 2. ζ-$(ET)_2(I_3)(I_5)$ (a) and ϵ-$(ET)_2(I_3)(I_8)_{0.5}$ (b) containing *mixed* ET-I_3^- sheets containing dimerized ET molecules and interweaving I_3^- anions. The ET donor molecules and I_3^- anions are linked by short S···S and S···I contacts that are less than the van der Waals sums (3.6 and 3.9 Å, respectively). However, the two salts possess different arrangements of the dimer units and stacking of the two independent ET molecules (A and B above).

Results and Discussion

Crystal Structure of ζ-$(ET)_2(I_3)(I_5)$. As shown in Figure 2a, ζ-$(ET)_2(I_3)(I_5)$ consists of sheets containing both ET molecules and I_3^- anions, as in the cases of ϵ-$(ET)_2(I_3)(I_8)_{0.5}$[7] and $(ET)_2(I_3)(TlI_4)$ (vide infra). These mixed ET–I_3^- layers contain stacks of dimerized ET molecules. In the case of ζ-$(ET)_2(I_3)(I_5)$ the stacking is along the crystallographic *b* axis. ET dimers in the stacks are tilted so as to create holes that accommodate I_3^- anions. The intermolecular S···S and S···I contact distances less than the van der Waals radii sums (3.6 and 3.9 Å, respectively) are indicated by thin lines in Figure 2a and are listed in Table V. As depicted in Figure 3, the mixed ET–I_3^- layers are separated by layers of nearly planar, V-shaped I_5^- anions in the ζ-phase. The

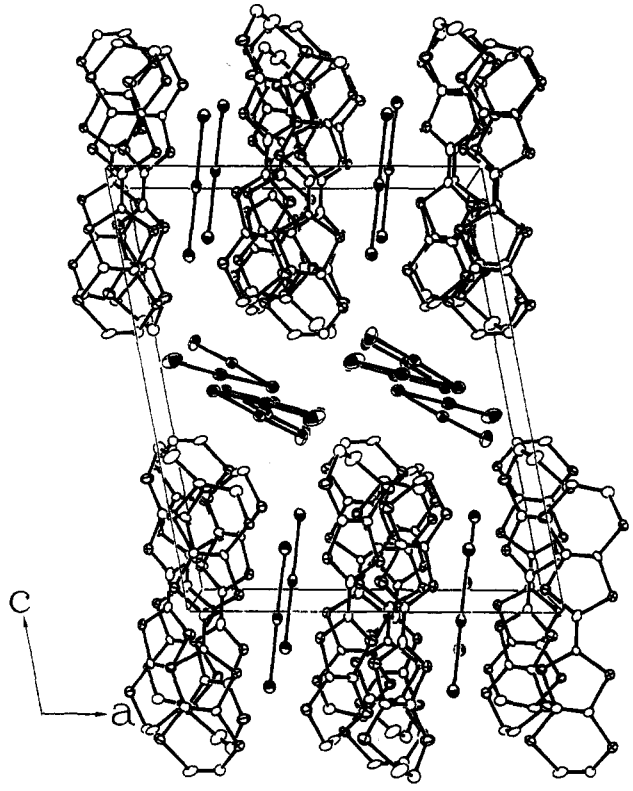

Figure 3. Mixed ET–I_3^- sheets in ζ-$(ET)_2(I_3)(I_5)$ separated along the crystallographic *c* axis by anion layers containing V-shaped I_5^- anions.

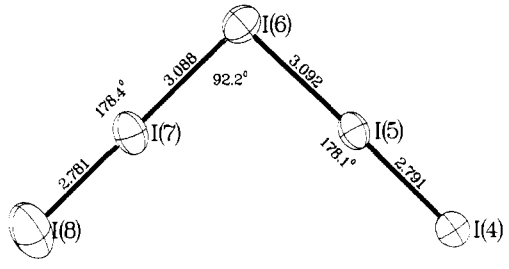

Figure 4. Geometry of the V-shaped I_5^- anions, nearly planar (within 0.03 Å) and symmetrical with noncrystallographic C_{2v} symmetry, similar to that observed in the CsI_5 salt.

structures of the ϵ- and ζ-phases are similar in that these materials contain mixed ET–I_3^- sheets separated by layers of planar anions (I_8^{2-} anions in the ϵ-phase), and there are similarly short S···S and S···I intermolecular contact distances within the ET–I_3^- sheets. Incidentally, these salts have the same crystallographic space group and possess similar unit cell constants. An important difference between the two salts is observed in the packing of the mixed ET–I_3^- layers. As displayed in Figure 2b, the dimerized ET molecules of ϵ-$(ET)_2(I_3)(I_8)_{0.5}$ are made up of two independent molecules (A and B). These dimer pairs are arranged in stacks along the crystallographic *a* axis, with adjacent pairs tipped in alternate directions (toward $+b$ and $-b$ axes). As shown in Figure 2a, however, the ζ-phase salt forms two types of dimer pairs, A–A and B–B. These two types of dimer pairs alternate along *b*, and all are tipped in the same direction. The interplanar spacing within an ET dimer is ~3.40 Å for the ζ-phase and ~3.61 Å for the ϵ-phase.[13]

Intramolecular distances and bond angles of ζ-$(ET)_2(I_3)(I_5)$ are listed in Table VI. The geometries of the I_3^- (Table VIA) and I_5^- anions (Table VIB and Figure 4) are consistent with those previously reported[3,12] with the formal charge of −1. In contrast to the superconducting β-$(ET)_2X$ salts ($X^- = I_3^-$, AuI_2^-, IBr_2^-) that contain nominally $ET^{0.5+}$, the formal charge on the ET molecules of ζ-$(ET)_2(I_3)(I_5)$ is +1. The HOMO of ET is heavily weighted on the TTF portion of ET.[21] In the HOMO, the C—S and C=C bonds of the TTF moiety are antibonding and bonding,

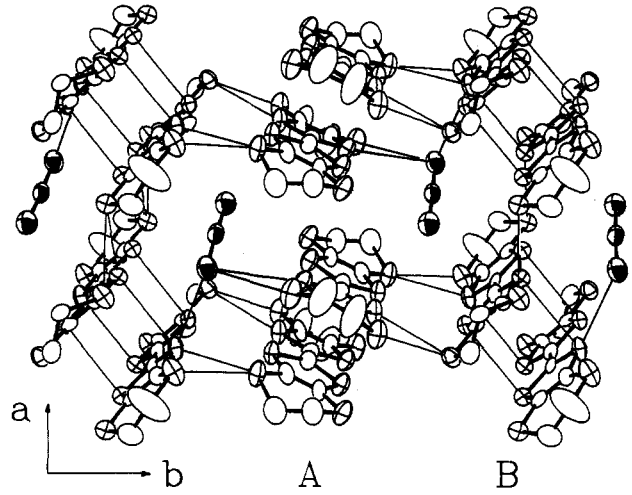

Figure 5. Mixed ET–I_3^- sheets in $(ET)_2(I_3)(TlI_4)$.

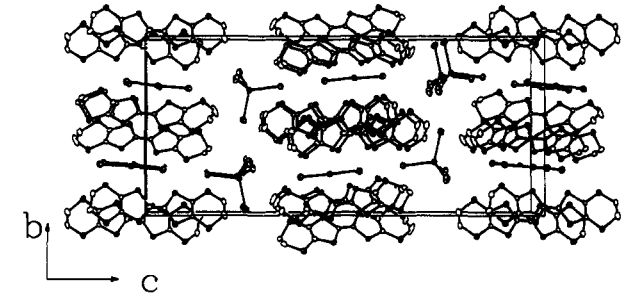

Figure 6. Projection of the structure of $(ET)_2(I_3)(TlI_4)$ along the *a* axis.

respectively.[21] Thus, oxidation of ET, which removes an electron from its HOMO, strengthens the C—S bonds but weakens the C=C bonds. Summarized in Table VII are the C—S and C=C bond lengths observed for the ET molecules with various degrees of formal oxidation. In general, the C—S and C=C bond lengths of the ET molecules in the ζ- and ϵ-phases are consistent with the conclusion that all the ET molecules in the two phases have the formal oxidation of +1.

Crystal Structure of $(ET)_2(I_3)(TlI_4)$. $(ET)_2(I_3)(TlI_4)$ also contains layers built up from ET molecules and I_3^- anions (see Figure 5). Again, dimers of ET molecules stack along the crystallographic *a* axis, and the holes between tilted dimers are filled with linear triiodide ions. Intermolecular S···S and S···I contacts less than the van der Waals radii sums (3.6 and 3.9 Å, respectively) are drawn as thin lines in Figure 5. All ET molecules of a given stack are crystallographically equivalent, unlike the cases of ζ-$(ET)_2(I_3)(I_5)$ and ϵ-$(ET)_2(I_3)(I_8)_{0.5}$, and adjacent stacks are unrelated by symmetry. The short intermolecular distances are all found in the stack formed by ET molecule B and between stacks. The shortest intradimer contact in stack A is 3.605 Å, nearly equal to the van der Waals radii sum.

The tetrahedral TlI_4^- anions are located between the mixed ET–I_3^- sheets, as shown in Figure 6. One iodine atom of TlI_4^- reaches into a pocket in the ET–I_3^- sheet and approaches an iodine atom of I_3^-, thereby leading to an I···I contact of 3.832 Å. The Tl–I bond lengths range from 2.736 to 2.757 Å, which are similar to the Tl–I length of 2.736–2.770 Å found in $CsTlI_4$.[20] The distortion from the tetrahedral geometry in TlI_4^- is less pronounced in the present compound than in the Cs^+ salt: The I–Tl–I angles are between 107.1 and 111.8° in $(ET)_2(I_3)(TlI_4)$ and between 105.1 and 117.6° in $CsTlI_4$.

The average C=C and C—S bond lengths of the TTF moiety found in the TlI_4^- salt are included in Table VII. In agreement with the +1 formal charge on the donor-radical cation, the C=C bonds are rather long, and the C—S bonds are short, but the large estimated errors (ca. 0.02 and 0.015 Å, respectively) preclude a definitive interpretation. Table VIII lists bond lengths and angles in $(ET)_2(I_3)(TlI_4)$.

Table V. Selected[a] Intermolecular Contact Distances (Å)

	dist	symmetry[b]		dist	symmetry
		A. ζ-$(ET)_2(I_3)(I_5)$			
		I···S Contact Distances			
I(1)–S(5)	3.685 (4)	$-0.5 + x, 0.5 - y, z$	I(3)–S(8)	3.780 (4)	$-0.5 + x, 0.5 - y, z$
I(3)–S(4)	3.782 (4)	$-0.5 + x, 0.5 - y, z$	I(4)–S(7)	3.731 (4)	$1 - x, -y, -z$
I(3)–S(16)	3.733 (4)	$-1 + x, y, 1 + z$			
		Intradimer S···S Contact Distances			
S(4)–S(6)	3.494 (5)	$2 - x, -y, -z$	S(11)–S(13)	3.450 (5)	$2 - x, 1 - y, -z$
S(12)–S(14)	3.461 (6)	$2 - x, 1 - y, -z$	S(15)–S(17)	3.549 (5)	$2 - x, 1 - y, -z$
		Interdimer S···S Contact Distances			
S(3)–S(15)	3.430 (5)	$0.5 + x, 0.5 - y, z$	S(6)–S(14)	3.417 (5)	$0.5 + x, 0.5 - y, z$
S(6)–S(18)	3.492 (6)	$0.5 + x, 0.5 - y, z$	S(7)–S(15)	3.416 (5)	$0.5 + x, 0.5 - y, z$
S(8)–S(16)	3.571 (6)	x, y, z			
		B. $(ET)_2(I_3)(TlI_4)$			
		I···S Contact Distances			
I(1)–S(7)	3.636 (5)	$-1 + x, y, z$	I(3)–S(5)	3.848 (5)	$-^1/_2 + x, {}^1/_2 - y, {}^1/_2 + z$
I(5)–S(13)	3.765 (5)	x, y, z	I(5)–S(5)	3.722 (5)	$-^1/_2 + x, {}^1/_2 - y, {}^1/_2 + z$
I(5)–S(1)	3.776 (5)	$-^1/_2 + x, {}^1/_2 - y, {}^1/_2 + z$	I(1)–S(15)	3.894 (4)	$-^1/_2 + x, {}^1/_2 - y, -^1/_2 + z$
		Intradimer S···S Contacts Distances			
S(1)–S(4)	3.605 (6)	$1 - x, 1 - y, -z$	S(11)–S(14)	3.504 (6)	$-x, -y, 1 - z$
S(12)–S(13)	3.468 (6)	$-x, -y, 1 - z$			
		Interdimer S···S Contact Distances			
S(2)–S(15)	3.456 (6)	$^1/_2 - x, -^1/_2 + y, {}^1/_2 - z$	S(6)–S(15)	3.506 (7)	$^1/_2 - x, -^1/_2 + y, {}^1/_2 - z$
S(8)–S(13)	3.525 (6)	$^1/_2 - x, -^1/_2 + y, {}^1/_2 - z$	S(8)–S(17)	3.378 (7)	$^1/_2 - x, -^1/_2 + y, {}^1/_2 - z$
S(12)–S(18)	3.553 (6)	$-1 - x, -y, 1 - z$	S(16)–S(18)	3.462 (6)	$-1 - x, -y, 1 - z$

[a] I···S and S···S intermolecular contact distances less than the sum of the van der Waals radii, 3.9 Å for I···S contacts and 3.6 Å for S···S contacts. [b] Symmetry operation for the second atom of the pair.

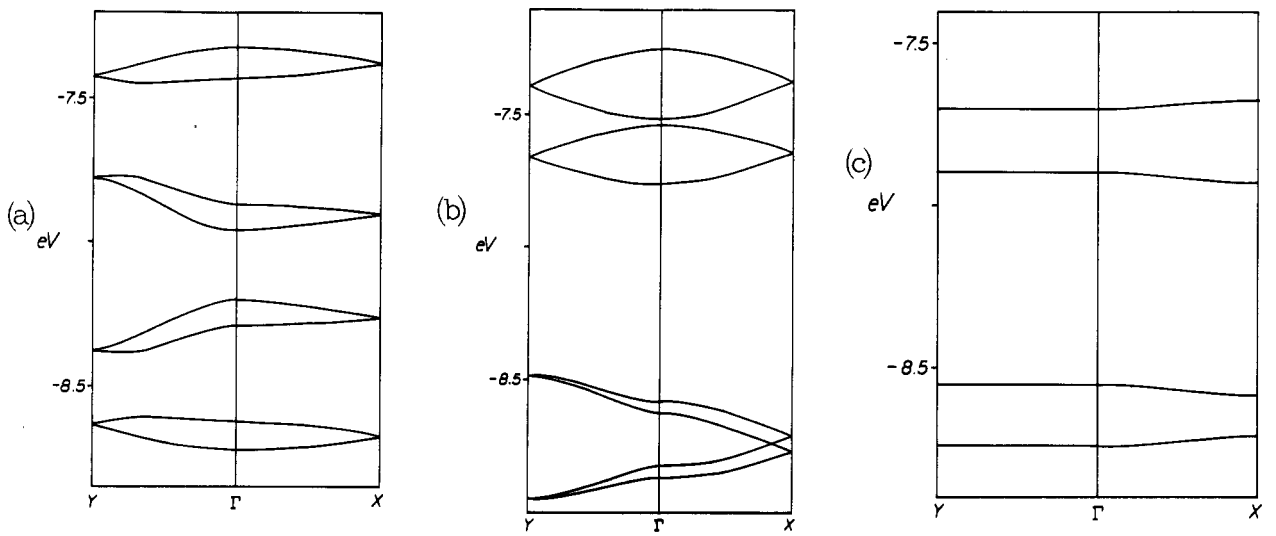

Figure 7. Band electronic structures of (a) ζ-$(ET)_2(I_3)(I_5)$, (b) ϵ-$(ET)_2(I_3)(I_8)_{0.5}$, and (c) $(ET)_2(I_3)(TlI_4)$ where $\Gamma = (0, 0)$ is the origin of the reciprocal space. For ϵ-$(ET)_2(I_3)(I_8)_{0.5}$ and $(ET)_2(I_3)(TlI_4)$ $X = (a^*/2, 0)$ and $Y = (0, b^*/2)$, while for ζ-$(ET)_2(I_3)(I_5)$ $X = (0, a^*/2)$ and $Y = (b^*/2, 0)$. With the formal oxidation of ET^+, the bottom four bands are fully occupied but the top four bands are completely empty in δ-$(ET)_2(I_3)(I_5)$ and ϵ-$(ET)_2(I_3)(I_8)_{0.5}$. However, in $(ET)_2(I_3)(TlI_4)$ the bottom two bands are fully occupied and the top two are completely empty.

Band Electronic Structure. Both the ζ- and ϵ-phases are metallic down to 1.7 K, as shown in Figure 1. The ζ- and ϵ-phases contain stacks made up of separated $(ET^+)_2$ dimers, so it is at first surprising that they are not semiconducting but metallic. Each mixed ET–I_3^- sheet of the ζ- and ϵ-phases has four $(ET^+)_2$ dimers and four I_3^- anions per unit cell. Parts a and b of Figure 7 show the tight-binding bands[22,23] calculated for ζ-$(ET)_2(I_3)(I_5)$ and ϵ-$(ET)_2(I_3)(I_8)_{0.5}$, respectively, within the framework of the extended Hückel method.[24] In Figure 7a or 7b, the eight bands, which derive largely from the HOMO's of eight ET molecules in each unit cell, are only weakly dispersive. With the formal oxidation of ET^+, there are eight electrons to fill the eight bands. Thus, when these bands are filled in a low-spin manner,[25] the bottom four bands become completely filled, and the rest of the four bands are empty.[27] Thus, both ζ-$(ET)_2(I_3)(I_5)$ and ϵ-$(ET)_2(I_3)(I_8)_{0.5}$ have band gaps and are not expected to be metals. This result is not unexpected since both the ζ- and ϵ-phases contain stacks of $(ET^+)_2$ dimers, but it is certainly not consistent with their obvious metallic properties. This apparent discrepancy may originate from the possibility that the ζ-$(ET)_2(I_3)(I_5)$ and ϵ-$(ET)_2(I_3)(I_8)_{0.5}$ salts are not as stoichiometric as implied by their chemical formulas but likely contain some kind of anion vacancies. Since these two salts are formed upon chemical oxidation by iodine vapor, it is plausible that some I_3^- sites of the mixed ET–I_3^- layers are occupied by I_2 instead of I_3^-. If this is the case, the net positive charge on the ET donor molecules is reduced, and the bottom of the conduction bands in Figure 7a,b will be partially filled, thereby

(27) Kato, R.; Kobayashi, H.; Kobayashi, A.; Mori, T.; Inokuchi, H., submitted for publication in *Chem. Lett.*

Table VI. Distances (Å) and Angles (deg) for ζ-$(ET)_2(I_3)(I_5)$

A. I_3^- Anion

Distances

I(1)–I(2)	2.932 (2)	I(2)–I(3)	2.889 (2)

Angle

I(2)–I(1)–I(3)	177.97 (5)

B. I_5^- Anion

Distances

I(4)–I(5)	2.792 (2)	I(5)–I(6)	3.091 (2)	I(6)–I(7)	3.087 (2)	I(7)–I(8)	2.781 (2)

Angles

I(4)–I(5)–I(6)	178.18 (5)	I(5)–I(6)–I(7)	92.23 (5)
I(6)–I(7)–I(8)	178.39 (7)		

C. ET Molecule A

Distances

S(1)–C(3)	1.704 (13)	S(1)–C(1)	1.718 (13)	S(2)–C(1)	1.725 (14)
S(2)–C(4)	1.738 (13)	S(3)–C(2)	1.698 (12)	S(3)–C(5)	1.759 (13)
S(4)–C(2)	1.713 (12)	S(4)–C(6)	1.722 (13)	S(5)–C(3)	1.752 (13)
S(5)–C(7)	1.830 (14)	S(6)–C(4)	1.715 (12)	S(6)–C(8)	1.800 (15)
S(7)–C(5)	1.714 (12)	S(7)–C(10)	1.802 (19)	S(7)–C(10)	1.816 (49)
S(8)–C(6)	1.748 (14)	S(8)–C(9)	1.865 (16)	C(1)–C(2)	1.414 (19)
C(3)–C(4)	1.367 (17)	C(5)–C(6)	1.366 (19)	C(7)–C(8)	1.527 (22)
C(9)–C(10A)	1.247 (50)	C(9)–C(10B)	1.412 (30)	C(10)–C(10)	0.860 (52)

Angles

C(3)–S(1)–C(1)	95.7 (7)	C(1)–S(2)–C(4)	95.9 (6)	C(4)–C(3)–S(5)	126.0 (10)	S(1)–C(3)–S(5)	115.7 (7)
C(2)–S(3)–C(5)	95.4 (6)	C(2)–S(4)–C(6)	93.9 (6)	C(3)–C(4)–S(6)	129.7 (10)	C(3)–C(4)–S(2)	114.9 (9)
C(3)–S(5)–C(7)	104.3 (6)	C(4)–S(6)–C(8)	98.4 (7)	S(6)–C(4)–S(2)	115.4 (7)	C(6)–C(5)–S(7)	130.0 (11)
C(5)–S(7)–C(10)	104.3 (8)	C(5)–S(7)–C(10)	97.0 (16)	C(6)–C(5)–S(3)	113.8 (10)	S(7)–C(5)–S(3)	116.3 (7)
C(6)–S(8)–C(9)	99.6 (7)	C(2)–C(1)–S(1)	123.7 (10)	C(5)–C(6)–S(4)	119.1 (10)	C(5)–C(6)–S(8)	124.6 (10)
C(2)–C(1)–S(2)	121.0 (9)	S(1)–C(1)–S(2)	115.2 (8)	S(4)–C(6)–S(8)	116.3 (8)	C(8)–C(7)–S(5)	114.5 (10)
C(1)–C(2)–S(3)	121.2 (9)	C(1)–C(2)–S(4)	121.3 (9)	C(7)–C(8)–S(6)	112.5 (11)	C(10A)–C(9)–S(8)	125.5 (26)
S(3)–C(2)–S(4)	117.5 (7)	C(4)–C(3)–S(1)	118.3 (10)	C(10B)–C(9)–S(8)	113.8 (14)	C(9)–C(10A)–S(7)	127.2 (37)
				C(9)–C(10B)–S(7)	117.6 (16)		

D. Molecule B

Distances

S(11)–C(13)	1.721 (14)	S(11)–C(11)	1.731 (14)	S(12)–C(11)	1.725 (14)
S(12)–C(14)	1.732 (13)	S(13)–C(12)	1.722 (14)	S(13)–C(15)	1.774 (14)
S(14)–C(12)	1.688 (15)	S(14)–C(16)	1.726 (15)	S(15)–C(13)	1.751 (13)
S(15)–C(17)	1.823 (14)	S(16)–C(14)	1.761 (14)	S(16)–C(18)	1.779 (17)
S(17)–C(15)	1.726 (14)	S(17)–C(19)	1.866 (19)	S(18)–C(16)	1.730 (15)
S(18)–C(20A)	1.779 (27)	S(18)–C(20B)	1.851 (43)	C(11)–C(12)	1.399 (21)
C(13)–C(14)	1.337 (20)	C(15)–C(16)	1.365 (20)	C(17)–C(18)	1.504 (22)
C(19)–C(20A)	1.248 (44)	C(19)–C(20B)	1.464 (37)	C(20A)–C(20B)	0.901 (42)

Angles

C(13)–S(11)–C(11)	95.7 (7)	C(11)–S(12)–C(14)	95.0 (7)	S(11)–C(13)–S(15)	114.2 (8)	C(13)–C(14)–S(12)	117.5 (11)
C(12)–S(13)–C(15)	94.6 (7)	C(12)–S(14)–C(16)	96.0 (7)	C(13)–C(14)–S(16)	127.8 (11)	S(12)–C(14)–S(16)	114.7 (8)
C(13)–S(15)–C(17)	102.2 (7)	C(14)–S(16)–C(18)	99.5 (7)	C(16)–C(15)–S(17)	128.2 (11)	C(16)–C(15)–S(13)	115.1 (10)
C(15)–S(17)–C(19)	98.5 (8)	C(16)–S(18)–C(20)	107.7 (11)	S(17)–C(15)–S(13)	116.6 (8)	C(15)–C(16)–S(14)	117.2 (11)
C(16)–S(18)–C(20)	92.1 (14)	C(20)–S(18)–C(20)	28.7 (13)	C(15)–C(16)–S(18)	124.7 (11)	S(14)–C(16)–S(18)	118.1 (9)
C(12)–C(11)–S(12)	123.2 (11)	C(12)–C(11)–S(11)	121.8 (10)	C(18)–C(17)–S(15)	113.0 (10)	C(17)–C(18)–S(16)	114.4 (11)
S(12)–C(10)–S(11)	114.9 (8)	C(11)–C(12)–S(14)	121.9 (11)	C(20A)–C(19)–S(17)	120.1 (22)	C(20B)–C(19)–S(17)	114.7 (15)
C(11)–C(12)–S(13)	121.1 (11)	S(14)–C(12)–S(13)	117.0 (9)	C(19)–C(20A)–S(18)	118.6 (20)	C(19)–C(20B)–S(18)	127.6 (30)
C(14)–C(13)–S(11)	116.8 (10)	C(14)–C(13)–S(15)	129.0 (11)				

leading to metallic properties. An I_3^- vacancy of up to ~2% cannot be discounted according to our single-crystal X-ray diffraction study.

From the viewpoint of our speculations concerning why ϵ-$(ET)_2(I_3)(I_8)_{0.5}$ and ζ-$(ET)_2(I_3)(I_5)$ are metallic, it is important to note the electrical properties of ϵ-$(ET)_2(I_3)(I_8)_{0.5}$ observed by Shibaeva et al.[5,7] and Merzhanov et al.[18] In their work ϵ-$(ET)_2(I_3)(I_8)_{0.5}$ was synthesized by chemical oxidation with a procedure different from ours. Initially, ϵ-$(ET)_2(I_3)(I_8)_{0.5}$ was reported to become a superconductor at about 3 K under ambient pressure.[5,18] In a later work, however, Shibaeva et al.[7] reported that ϵ-$(ET)_2(I_3)(I_8)_{0.5}$ is not a metal but a semiconductor. As already stated, the crystal structures of ϵ-$(ET)_2(I_3)(I_8)_{0.5}$ as determined by Shibaeva et al.[7] and by us are in excellent agreement. Certainly, then, the semiconducting behavior of this salt observed by Shibaeva et al.[7] agrees with the prediction of our band electronic structure calculations. The apparently conflicting electrical properties of ϵ-$(ET)_2(I_3)(I_8)_{0.5}$ are understandable if chemical oxidation introduces nonstoichiometry and if the extent of nonstoichiometry alters the electrical properties of a given salt from semiconducting to metallic or even to superconducting.

The $(ET)_2(I_3)(TlI_4)$ salt obtained by *electrocrystallization* is observed to be semiconducting in agreement with the structural feature that this salt contains mixed ET–I_3^- layers made of $(ET^+)_2$ dimers. Shown in Figure 7c is the band electronic structure calculated for $(ET)_2(I_3)(TlI_4)$, which has two $(ET^+)_2$ units per unit cell and hence has the four bands derived from the HOMO of ET. These bands are much less dispersive than the corresponding ones in ζ-$(ET)_2(I_3)(I_5)$ and ϵ-$(ET)_2(I_3)(I_8)_{0.5}$. With four electrons to occupy these bands, the bottom two bands are completely filled, leaving the top two bands empty. Therefore, in agreement with experiment, $(ET)_2(I_3)(TlI_4)$ is not predicted to be a metal. Thus, the $(ET)_2(I_3)(TlI_4)$ salt must be highly stoichiometric, as indicated by its chemical formula.

Concluding Remarks

Chemical oxidation of ET in benzonitrile by iodine vapor leads to a new salt, ζ-$(ET)_2(I_3)(I_5)$, that consists of mixed ET–I_3^- sheets

Table VII. Average Intramolecular Distances (Å)[a] for Various Observed Charges on the ET Molecule

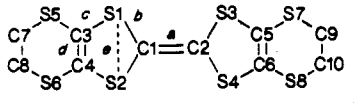

species	*a*	*b*	*c*	*d*	*e*	ref
ET^0	1.32	1.76	1.75	1.33	2.94	14
$ET^{+1/2}$	1.366	1.742	1.756	1.356	2.945	2, 3, 5, *b*
$ET^{+2/3}$	1.373	1.730	1.747	1.353	2.925	15, *b*
ET^{+1}	1.38	1.72	1.73	1.37	2.91	16
ζ-$(ET)_2(I_3)(I_5)$						
ET molecule A	1.41	1.71	1.73	1.37	2.91	this work
ET molecule B	1.40	1.72	1.74	1.35	2.91	
ϵ-$(ET)_2(I_3)(I_8)_{0.5}$						
ET molecule A	1.43	1.71	1.74	1.35	2.90	this work
ET molecule B	1.37	1.73	1.74	1.33	2.91	and ref 7
$(ET)_2(TlI_4)I_3$						
ET molecule A	1.35	1.73	1.72	1.36	2.91	this work
ET molecule B	1.37	1.72	1.74	1.36	2.91	

[a] Standard deviations as derived from averaging are ~0.01 Å. [b] Standard deviations from averaging are ~0.005 Å.

separated by layers of I_5^- ions. As in ϵ-$(ET)_2(I_3)(I_8)_{0.5}$, also obtained by chemical oxidation, each mixed ET–I_3^- sheet of ζ-$(ET)_2(I_3)(I_5)$ contains stacks of $(ET^+)_2$ dimers. Electrical conductivity measurements by the four-probe technique show that ζ-$(ET)_2(I_3)(I_5)$ and ϵ-$(ET)_2(I_3)(I_8)_{0.5}$ are metallic down to 1.7 K. However, these two salts are not bulk superconductors down to 0.5 K according to our measurements of rf field penetration depth. Our tight-binding-band calculations indicate that ζ-$(ET)_2(I_3)(I_5)$, ϵ-$(ET)_2(I_3)(I_8)_{0.5}$, and $(ET)_2(I_3)(TlI_4)$ are not metallic but semiconducting, provided that these salts are as stoichiometric as suggested by their chemical formulas. Thus, the metallic properties of the ϵ- and ζ-phase salts most likely originate from some kind of anion vacancy. If some I_3^- sites of mixed ET–I_3 layers are occupied by I_2, the conduction bands of the stoichiometric ζ- and ϵ-phases will be partially filled and responsible for their metallic properties. Further studies are necessary to confirm the presence of anion vacancies in these salts. In conclusion, it appears that the electrochemical synthesis of charge-transfer salts containing mixed ET–I_3^- sheets under the conditions for slow crystal growth (i.e., low current density on the order of 1–5 μA) leads to stoichiometric products opposed to the chemical oxidation

Table VIII. Distances (Å) and Angles (deg) for $(ET)_2(I_3)(TlI_4)$

A. I_3^- Anion

Distances

I(5)–I(6)	2.914 (2)	I(6)–I(7)	2.916 (2)

Angle

I(5)–I(6)–I(7)	177.95 (6)

B. TlI_4^- Anion

Distances

Tl–I(1)	2.757 (2)	Tl–I(2)	2.746 (2)	Tl–I(3)	2.736 (2)	Tl–I(4)	2.750 (2)

Angles

I(1)–Tl–I(2)	109.90 (5)	I(1)–Tl–I(3)	107.07 (5)	I(1)–Tl–I(4)	107.95 (5)
I(2)–Tl–I(3)	111.79 (5)	I(2)–Tl–I(4)	108.29 (6)	I(3)–Tl–I(4)	111.76 (6)

C. ET Molecule A

Distances

S(1)–C(1)	1.725 (15)	S(1)–C(3)	1.726 (15)	S(2)–C(1)	1.712 (15)
S(2)–C(4)	1.740 (15)	S(3)–C(2)	1.754 (16)	S(3)–C(5)	1.719 (15)
S(4)–C(2)	1.728 (15)	S(4)–C(6)	1.714 (15)	S(5)–C(3)	1.738 (14)
S(5)–C(7)	1.786 (21)	S(6)–C(4)	1.753 (15)	S(6)–C(8)	1.798 (20)
S(7)–C(5)	1.723 (15)	S(7)–C(9)	1.791 (18)	S(8)–C(6)	1.740 (15)
S(8)–C(10)	1.794 (18)	C(1)–C(2)	1.347 (20)	C(3)–C(4)	1.345 (18)
C(5)–C(6)	1.384 (18)	C(7)–C(8)	1.294 (24)	C(9)–C(10)	1.402 (22)

Angles

C(1)–S(1)–C(3)	96.1 (7)	C(1)–S(2)–C(4)	95.6 (7)	S(5)–C(3)–C(4)	127.4 (12)	S(2)–C(4)–S(6)	115.9 (9)
C(2)–S(3)–C(5)	96.7 (7)	C(2)–S(4)–C(6)	96.5 (8)	S(2)–C(4)–C(3)	116.9 (11)	S(6)–C(4)–C(3)	127.1 (12)
C(3)–S(5)–C(7)	102.6 (9)	C(4)–S(6)–C(8)	101.3 (9)	S(3)–C(5)–S(7)	115.3 (8)	S(3)–C(5)–C(6)	115.5 (12)
C(5)–S(7)–C(9)	102.4 (8)	C(6)–S(8)–C(10)	99.6 (8)	S(7)–C(5)–C(6)	129.0 (12)	S(4)–C(6)–S(8)	115.4 (9)
S(1)–C(1)–S(2)	115.0 (9)	S(1)–C(1)–C(2)	122.5 (12)	S(4)–C(6)–C(5)	117.4 (11)	S(8)–C(6)–C(5)	127.2 (12)
S(2)–C(1)–C(2)	122.5 (12)	S(3)–C(2)–S(4)	113.8 (10)	S(5)–C(7)–C(8)	123.6 (18)	S(6)–C(8)–C(7)	129.7 (17)
S(3)–C(2)–C(1)	122.0 (12)	S(4)–C(2)–C(1)	124.0 (13)	S(7)–C(9)–C(10)	119.3 (15)	S(8)–C(10)–C(9)	118.9 (14)
S(1)–C(3)–S(5)	116.3 (9)	S(1)–C(3)–C(4)	116.3 (11)				

D. ET Molecule B

Distances

S(11)–C(11)	1.731 (14)	S(11)–C(13)	1.718 (15)	S(12)–C(11)	1.724 (14)
S(12)–C(14)	1.726 (14)	S(13)–C(12)	1.726 (14)	S(13)–C(15)	1.753 (15)
S(14)–C(12)	1.709 (14)	S(14)–C(16)	1.766 (15)	S(15)–C(13)	1.770 (14)
S(15)–C(17)	1.789 (18)	S(16)–C(14)	1.753 (15)	S(16)–C(18)	1.804 (15)
S(17)–C(15)	1.720 (15)	S(17)–C(19)	1.727 (22)	S(18)–C(16)	1.736 (15)
S(18)–C(20)	1.814 (17)	C(11)–C(12)	1.373 (18)	C(13)–C(14)	1.357 (18)
C(15)–C(16)	1.349 (18)	C(17)–C(18)	1.503 (21)	C(19)–C(20)	1.404 (24)

Angles

C(11)–S(11)–C(13)	95.3 (7)	C(11)–S(12)–C(14)	95.6 (7)	S(15)–C(13)–C(14)	129.8 (12)	S(12)–C(14)–S(16)	117.7 (8)
C(12)–S(13)–C(15)	96.8 (7)	C(12)–S(14)–C(16)	95.7 (7)	S(12)–C(14)–C(13)	116.5 (12)	S(16)–C(14)–C(13)	125.8 (12)
C(13)–S(15)–C(17)	101.8 (7)	C(14)–S(16)–C(18)	99.3 (7)	S(13)–C(15)–S(17)	116.5 (9)	S(13)–C(15)–C(16)	115.1 (12)
C(15)–S(17)–C(19)	103.5 (9)	C(16)–S(18)–C(20)	102.4 (8)	S(17)–C(15)–C(16)	128.4 (12)	S(14)–C(16)–S(18)	114.0 (9)
S(11)–C(11)–S(12)	115.2 (8)	S(11)–C(11)–C(12)	121.2 (11)	S(14)–C(16)–C(15)	117.2 (12)	S(18)–C(16)–C(15)	128.8 (12)
S(12)–(11)–C(12)	123.6 (11)	S(14)–C(12)–C(11)	124.7 (11)	S(15)–C(17)–C(18)	114.8 (12)	S(16)–C(18)–C(17)	112.4 (11)
S(13)–C(12)–C(11)	120.0 (11)	S(13)–C(12)–S(14)	115.2 (8)	S(17)–C(19)–C(20)	127.5 (17)	S(18)–C(20)–C(19)	119.8 (14)
S(11)–C(13)–S(15)	112.8 (8)	S(11)–C(13)–C(14)	117.4 (11)				

process and that the chemical oxidation procedure described herein offers a method for the production of metallic conducting materials from otherwise stoichiometric and nonconducting systems.

Acknowledgment. Work at Argonne National Laboratory is sponsored by the U.S. Department of Energy (DOE), Office of Basic Energy Sciences, Division of Materials Sciences, under Contract W-31-109-ENG-38. K.L.K., M.A.F., and K.S.W. are student research participants coordinated by the Argonne Division of Educational Programs from the University of Wisconsin, River Falls, WI, Indiana University, Indiana, PA, and St. Michael's College, Winooski, VT, respectively. Research at North Carolina State University was in part supported by DOE, Office of Basic Sciences, Division of Materials Sciences, under Grant DE-FG05-86ER45259. M.-H.W. is a participant in the Faculty Research Program, sponsored by Argonne Division of Educational Programs with funding provided by DOE. The authors express their appreciation for computing time on the ER-Cray X-MP computer, made available by DOE.

Registry No. ET, 66946-48-3; $(ET)_2(I_3)(I_5)$, 107798-36-7; $(ET)(I_3)(TlI_4)$, 107798-35-6.

Supplementary Material Available: Tables of the refined anisotropic thermal parameters for all non-hydrogen atoms of ζ-$(ET)_2(I_3)(I_5)$, ϵ-$(ET)_2(I_3)(I_8)_{0.5}$, and $(ET)_2(I_3)(TlI_4)$ (Tables IX, XIII, and XIV) and listings of experimental parameters for the X-ray diffraction study and final positional and thermal parameters for ϵ-$(ET)_2(I_3)(I_8)_{0.5}$ (Tables XI and XII) (5 pages); lists of observed and calculated structure factors for ζ-$(ET)_2(I_3)(I_5)$ and $(ET)_2(I_3)(TlI_4)$ (Tables X and XV) (48 pages). Ordering information is given on any current masthead page.

Contribution from the Department of Chemistry and Molecular Structure Center, Indiana University, Bloomington, Indiana 47405

Tris(*N*,*N*′-dimethylethylenediaminato)dimolybdenum and Tris(*N*,*N*′-dimethylethylenediaminato)ditungsten. A Comparison of Eclipsed and Staggered Triple Bonds, $\sigma^2\pi^4$, between Molybdenum and Tungsten Atoms in $X_3M{\equiv}MX_3$ Compounds

Timothy P. Blatchford, Malcolm H. Chisholm,* and John C. Huffman

Received September 10, 1986

The compounds $M_2(MeNCH_2CH_2NMe)_3$ have been prepared by metathetic reactions involving 1,2-$M_2Cl_2(NMe_2)_4$ and Li_2-[$MeNCH_2CH_2NMe$] compounds for M = Mo and W. Addition of the diamine $Me(H)NCH_2CH_2N(H)Me$ (>3 equiv) to hydrocarbon solutions of either $M_2(O\text{-}t\text{-}Bu)_6$ or $M_2(NMe_2)_6$ in the presence of a trace amount of HBr also gives M_2-$(MeNCH_2CH_2NMe)_3$ compounds. The latter compounds have been characterized by a variety of physical techniques including single-crystal X-ray studies. The diaminato ligands span the M≡M bond such that the central M_2N_6 moiety is nearly eclipsed, having N–M–M–N torsion angles in the range 10–14°. The M–M distances are 2.190 (1) Å (M = Mo) and 2.264 (1) Å (M = W), shorter by 0.02 and 0.03 Å than the M–M distances in the related $M_2(NMe_2)_6$ compounds. The origin of this shortening is discussed and attributed to the presence of the bridging ligands rather than to differences in the electronic nature of the M≡M bond as a function of the eclipsed vs. staggered conformation of the central M_2N_6 unit. Cell dimensions at −175 °C for $Mo_2(MeNCH_2CH_2NMe)_3$: a = 12.036 (3) Å, b = 9.480 (3) Å, c = 8.783 (2) Å, α = 107.94 (3)°, β = 100.56 (2)°, γ = 100.65 (2)°, cell volume = 905.55 (9) Å^3, Z = 2, d_{calcd} = 1.651 g cm^{-3}, $R(F)$ = 0.0247, $R_w(F)$ = 0.0408, space group $P\bar{1}$. Cell dimensions for $W_2(MeNCH_2CH_2NMe)_3$ at −161 °C: a = 11.869 (3) Å, b = 9.477 (2) Å, c = 8.841 (2) Å, α = 107.92 (1)°, β = 99.61 (1)°, γ = 98.99 (1)°, cell volume = 909.76 (10) Å^3, Z = 2, d_{calcd} = 2.286 g cm^{-3}, $R(F)$ = 0.0475, $R_w(F)$ = 0.0494, space group $P\bar{1}$.

Introduction

Compounds of types **1** and **2** have proven to be quite extensive.[1] These compounds contain metal–metal triple bonds unsupported by bridging ligands, where the triple bond is viewed as being

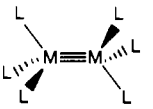

1

L = NR_2,[1a] OR,[1b] R,[1c] SAr[1d]

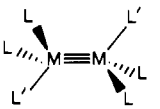

2

L = NR_2; L′ = alkyl,[1e] aryl,[1f] Cl,[1g] OR[1h]

L = OR; L′ = OR[1h]

L = OR; L = R[1i]

L = R; L′ = OR, NR_2, Br[1k]

composed of one σ and two equivalent π components [$\sigma(d_{z^2}\text{–}d_{z^2})$, $\pi(d_{xz},d_{yz}\text{–}d_{xz},d_{yz})$].[2] In all structural studies to date, M_2L_6 and $M_2L'_2L_4$ compounds adopt staggered, D_{3d}, ethane-like core conformations. In all of the early work this geometry was assumed to arise because of steric constraints since a metal–metal triple bond of configuration $\sigma^2\pi^4$ should be cylindrical for any molecule having a C_3 axis of symmetry coincident with the M–M bond.

Albright and Hoffmann's[3] provocative claim that these M_2L_6 (M≡M) dimers "should prefer the eclipsed conformation" has

(1) (a) M = Mo: Chisholm, M. H.; Cotton, F. A.; Frenz, B. A.; Reichert, W. W.; Shive, L. W.; Stults, B. R. *J. Am. Chem. Soc.* **1976**, *98*, 4469. M = W: Chisholm, M. H.; Cotton, F. A.; Extine, M. W.; Stults, B. R. *J. Am. Chem. Soc.* **1976**, *98*, 4477. (b) M = Mo: Chisholm, M. H.; Cotton, F. A.; Murillo, C. A.; Reichert, W. W. *Inorg. Chem.* **1977**, *16*, 1801. M = W: Akiyama, M.; Chisholm, M. H.; Cotton, F. A.; Extine, M. W.; Haitko, D. A.; Little, D.; Fanwick, P. E. *Inorg. Chem.* **1979**, *18*, 2266. (c) M = Mo: Huq, F.; Mowat, W.; Shortland, A.; Skapski, A. C.; Wilkinson, G. *J. Chem. Soc., Chem. Commun.* **1971**, 1079. M = W: Chisholm, M. H.; Cotton, F. A.; Extine, M. W.; Stults, B. R. *Inorg. Chem.* **1976**, *15*, 2252. (d) M = Mo: Chisholm, M. H.; Corning, J. F.; Huffman, J. C. *J. Am. Chem. Soc.* **1983**, *105*, 5924. M = W: Chisholm, M. H.; Corning, J. F.; Folting, K.; Huffman, J. C. *Polyhedron* **1985**, *4*, 383. (e) M = Mo and W: Chisholm, M. H.; Haitko, D. A.; Huffman, J. C. *J. Am. Chem. Soc.* **1981**, *103*, 4046. (f) Chetcuti, M. J.; Chisholm, M. H.; Folting, K.; Haitko, D. A.; Huffman, J. C.; Janos, J. *J. Am. Chem. Soc.* **1983**, *105*, 1163. (g) Akiyama, M.; Chisholm, M. H.; Cotton, F. A.; Extine, M. W.; Murillo, C. A. *Inorg. Chem.* **1977**, *16*, 2407. (h) Chisholm, M. H.; Garman, J., results submitted for publication. (i) M = Mo: Chisholm, M. H.; Tatz, R. J. *Organometallics*, in press. Chisholm, M. H.; Eichhorn, B. W.; Folting, K.; Huffman, J. C.; Tatz, R. J. *Organometallics*, in press. (j) M = Mo: Chisholm, M. H.; Corning, J. F.; Huffman, J. C. *Inorg. Chem.* **1984**, *23*, 754. (k) M = Mo: Chisholm, M. H.; Folting, K.; Huffman, J. C.; Rothwell, I. P. *Organometallics* **1982**, *1*, 251.

(2) Electronic description via SCF-Xα and photoelectron spectra: (a) Cotton, F. A.; Stanley, G. G.; Kalbacher, B. J.; Green, J. C.; Seddon, E.; Chisholm, M. H. *Proc. Natl. Acad. Sci. USA* **1977**, *74*, 3109. (b) Bursten, B. E.; Cotton, F. A.; Green, J. C.; Seddon, E. A.; Stanley, G. G. *J. Am. Chem. Soc.* **1980**, *102*, 4579.

(3) Albright, T. A.; Hoffmann, R. *J. Am. Chem. Soc.* **1978**, *100*, 7736.

0020-1669/87/1326-1920$01.50/0